

Spin-phonon interaction in yttrium iron garnet

Kevin S. Olsson^{1,2,*}, Jeongheon Choe^{1,3,*}, Martin Rodriguez-Vega^{1,3,4,†}, Guru Khalsa⁵, Nicole A. Benedek^{1,3,7,‡},
Jiaming He^{6,7}, Bin Fang^{1,3}, Jianshi Zhou^{3,6,7}, Gregory A. Fiete^{4,8} and Xiaoqin Li^{1,3,7,‡}

¹Department of Physics, Center of Complex Quantum Systems, The University of Texas at Austin, Austin, Texas 78712, USA

²Department of Computer and Electrical Engineering, University of Maryland, College Park, Maryland 20740, USA

³Center for Dynamics and Control of Materials, The University of Texas at Austin, Austin, Texas 78712, USA

⁴Department of Physics, Northeastern University, Boston, Massachusetts 02115, USA

⁵Department of Materials Science and Engineering, Cornell University, Ithaca, New York 14853, USA

⁶Department of Mechanical Engineering, The University of Texas at Austin, Austin, Texas 78712, USA

⁷Texas Materials Institute, The University of Texas at Austin, Austin, Texas 78712, USA

⁸Department of Physics, Massachusetts Institute of Technology, Cambridge, Massachusetts 02139, USA



(Received 16 March 2021; revised 14 May 2021; accepted 17 May 2021; published 1 July 2021)

Spin-phonon interaction is an important channel for spin and energy relaxation in magnetic insulators. Understanding this interaction is critical for developing magnetic insulator-based spintronic devices. Quantifying this interaction in yttrium iron garnet (YIG), one of the most extensively investigated magnetic insulators, remains challenging because of the large number of atoms in a unit cell. Here, we report temperature-dependent and polarization-resolved Raman measurements in a YIG bulk crystal. We first classify the phonon modes based on their symmetry. We then develop a modified mean-field theory and define a symmetry-adapted parameter to quantify spin-phonon interaction in a phonon-mode specific way in YIG. Based on this improved mean-field theory, we discover a positive correlation between the spin-phonon interaction strength and the phonon frequency.

DOI: [10.1103/PhysRevB.104.L020401](https://doi.org/10.1103/PhysRevB.104.L020401)

I. INTRODUCTION

Magnetic insulators are of considerable interest in spintronics due to their minimal spin damping [1–3]. This low damping originates in part from the absence of low-energy electronic excitations, leaving the spins to interact primarily with other spins (magnons) and the lattice (phonons). Beyond their role in spin-excitation damping, interactions between the magnons and phonons play a crucial role in developing devices based on thermally driven spin transport [4–6], spin pumping through hybrid spin-lattice excitations [7], and magnon cavity quantum electrodynamics [8,9]. Of various magnetic insulators explored for spintronic devices, yttrium iron garnet (YIG): $Y_3Fe_5O_{12}$ is the most widely investigated due to its remarkably low spin damping and its high transition temperature of 560 K [10,11]. While *ab initio* studies have some progress at describing spin-wave phenomena [12,13], extracting the spin-phonon interaction (SPI) of YIG remains difficult due to its massive unit cell [160 atoms as in inset of Fig. 1(a)].

The SPI in YIG has been investigated through different types of experiments. Brillouin light scattering and spin Seebeck transport measurements of YIG have examined the interactions of magnons and phonons through quasiparticle hybridization [14–17]. Other studies have touched upon

the SPI by measuring the magnon-phonon energy relaxation length and time [4,18–20]. However, no study provides a direct and quantitative measurement of the strength of the SPI in YIG in a phonon-mode specific way. Without knowing the SPI strength, it is difficult to develop accurate models of spin relaxation in YIG or compare YIG to other magnetic insulators for device development.

Here we report Raman spectroscopy studies of optical phonons in a YIG bulk crystal. By analyzing their symmetry properties and temperature-dependent phonon frequency shift, we investigate if SPI changes systematically for each phonon mode. We determine that the complex unit cell precludes a direct correlation between symmetry or frequency of a phonon mode with the conventional λ model of the SPI strength [21–23]. By developing a mean-field model and defining a parameter to describe SPI strength, we observe a correlation between this mean-field SPI parameter and phonon frequency. These results provide crucial information and advance the understanding of how magnons and phonons interact in YIG.

II. EXPERIMENT

YIG ($Y_3Fe_5O_{12}$) is an insulating ferrimagnet (FiM) with Curie temperature $T_C = 570$ K [24,25]. YIG crystals exhibit symmetries described by cubic space group $Ia\bar{3}d$ (No. 230) and point group O_h at the Γ point [26–28]. Inversion symmetry present in O_h implies that the phonon modes show mutually exclusive infrared and Raman activity. The possible Raman irreducible representations in O_h are either T_{2g} , E_g ,

*These authors contributed equally to this work.

†rodriguezvega@utexas.edu

‡elaineli@physics.utexas.edu

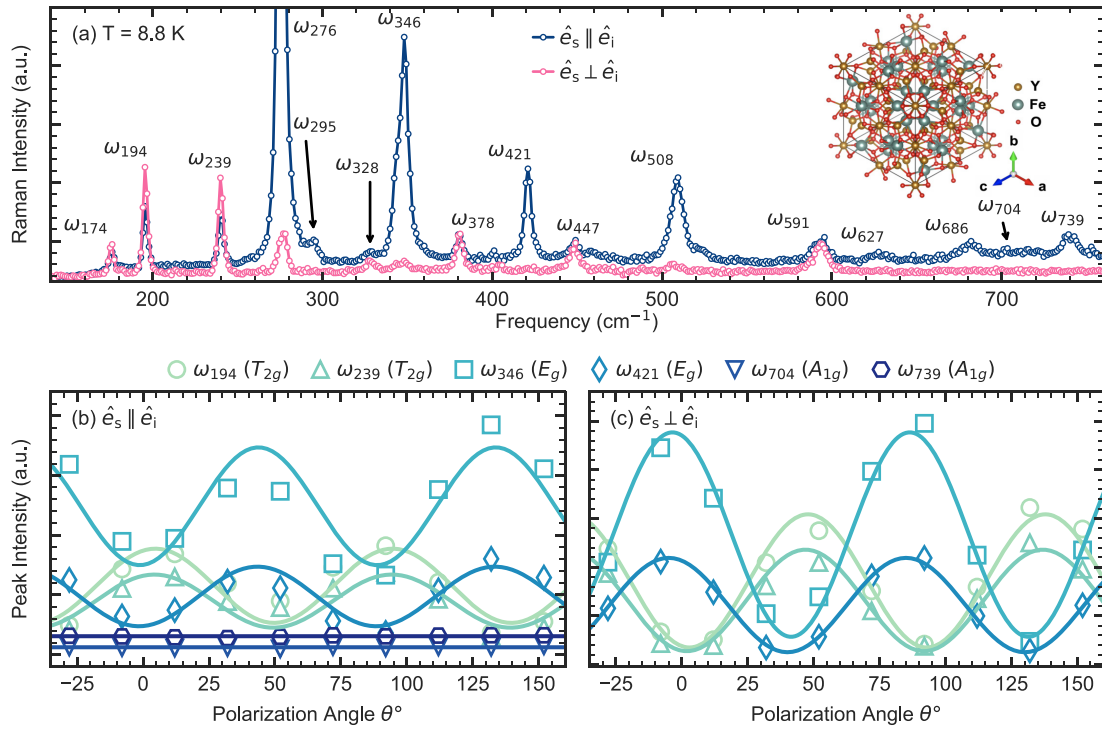


FIG. 1. (a) Raman spectra taken with $\hat{e}_s \parallel \hat{e}_i$ (colinear) and $\hat{e}_s \perp \hat{e}_i$ (crossed) polarization configurations at 8.8 K. Solid lines connect data points for clarity. Inset shows the YIG crystal structure viewed along the [111] direction. (b), (c) Angle-dependent intensities of the representative A_{1g} , E_g , and T_{2g} modes. The spectra were obtained by keeping incident polarization fixed. Panels (b) and (c) refer to colinear and crossed polarization configurations, respectively. The fit curves follow theoretical predictions from crystal lattice symmetry.

or A_{1g} . The crystal structure is composed of Y atoms occupying the 24c Wyckoff sites, Fe ions in the 16a and 24d positions, and O atoms in the 96h sites. The conventional unit cell has 8 formula units, with 24 Y ions, 40 Fe ions, and 96 O ions for a total of 160 atoms.

Raman measurements were taken with a 532-nm laser incident on a bulk YIG single crystal with [001] oriented along the surface normal. The sample measured approximately 5 mm \times 3 mm \times 1 mm and was grown using the traveling-solvent floating-zone method in an infrared-heated image furnace [29]. The scattered light was collected in a backscattering geometry and directed to a diffraction grating-based spectrometer. The observed optical phonon modes in the Raman spectra agree with previous measurements of YIG [30,31]. Low-temperature measurements from 8.8 to 313.65 K were performed in a closed-loop cryostat, and high-temperature measurements from 313.65 to 631.95 K were performed with a ceramic heater. Between each temperature, the sample was allowed to equilibrate for 15 min or longer. The laser spot sizes and powers were 0.8 μ m and 4 mW, and 1.3 μ m and 6 mW, for the high and low-temperature measurement sets, respectively. A saturating magnetic field was applied in the sample plane for all measurements. Due to constraints of the experiment systems, low-temperature measurements used a 300-mT saturating field, and the high-temperature measurements used a 50-mT saturating field. As both fields were above the saturating field, typically ~ 10 s of mT, this difference did not noticeably affect the magnetic ordering of YIG or the Raman spectra [32,33].

Raman spectra were collected with a fixed polarization (\hat{e}_i) and normal incidence on the sample. Figure 1(a) shows the spectra collect for the scattered light polarization (\hat{e}_s) parallel and perpendicular to \hat{e}_i , at low temperature (8.8 K). Phonon modes of different symmetries scatter light with different polarizations. Figures 1(b) and 1(c) show the intensity of the Raman signal from the scattered light as it passed through a linear polarizer, with the polarization axis rotated in steps of 20° from -28° to 152° , with 0° corresponding to aligned parallel with the [110] crystal axis. Based on the results, the phonons are categorized with their respective irreducible representations: T_{2g} , E_g , or A_{1g} .

The temperature dependence of the phonon frequencies was determined by fitting with a Lorentzian function and extracting the central frequencies. We plot the measured Raman spectra for one T_{2g} mode at three different representative temperatures; 8.8, 313.65, and 632 K in Figs. 2(a)–2(c), respectively. At low temperatures (e.g., 8.8 K), the low thermal population of the phonons reduces the Raman intensity. In contrast, the phonon modes exhibit a broader linewidth at high temperatures due to increased phonon-phonon and phonon-magnon scattering, which lowers the peak intensity. Consequently, the temperature-dependent frequency was only measurable for a subset of the observed phonons. The temperature dependence of the peak frequencies for the two modes is shown in Figs. 2(d) and 2(e). The temperature dependence of peak frequencies of all the measurable phonon modes can be found in Supplemental Material [34].

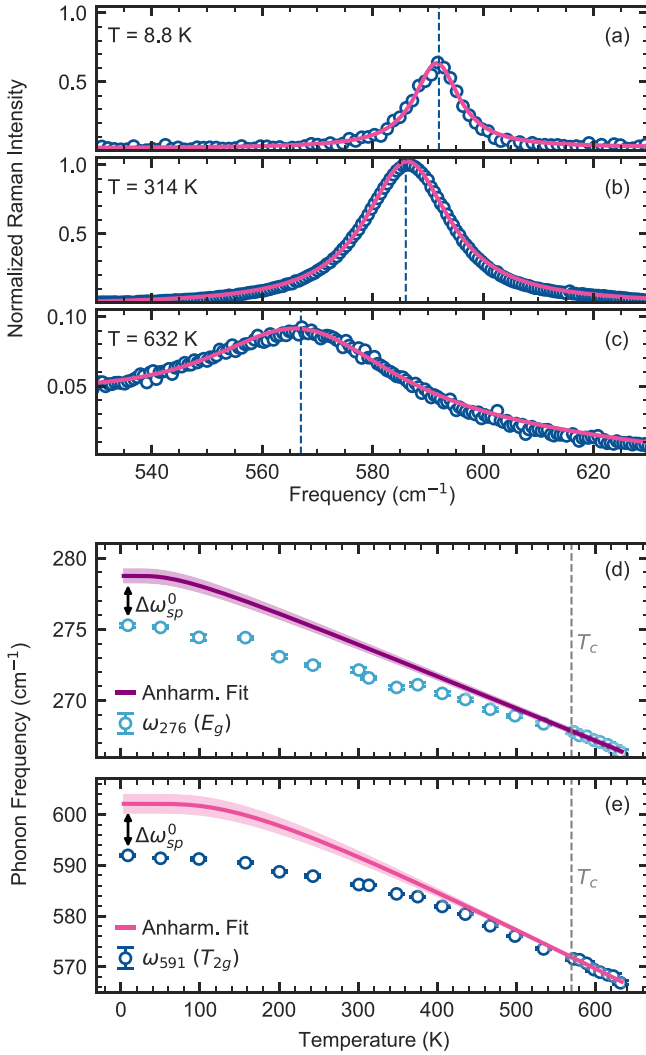


FIG. 2. (a)–(c) Example spectra for different temperatures, normalized to the peak intensity at 314 K. Solid lines are Lorentzian fits with a linear offset to account for the background. Vertical dashed lines indicate the peak positions. (d), (e) Temperature dependence of ω_{276} and ω_{591} phonon frequencies, which have symmetries T_{2g} and E_g , respectively. The solid curves correspond to the anharmonic phonon-phonon scattering fit, which is based on fitting to data only above the temperature T_c . The deviation from the anharmonic curve (black arrow) reflects the corresponding spin-phonon coupling strength, λ , given in Eq. (2).

III. RESULTS

In the absence of spin order above the transition temperature (i.e., 559 K for YIG), the temperature dependence of the optical phonon frequency ω_p is determined by anharmonic effects, i.e., phonon-phonon scattering. Well below the melting points, three-phonon scattering dictates the temperature dependence of ω_p as follows:

$$\omega_p(T) = \omega_p(0) - A \left(1 + \frac{2}{\exp[x] - 1} \right), \quad (1)$$

where $\omega_p(0)$ is the zero-temperature phonon frequency, A is a coefficient related to the three-phonon scattering strength, and $x = \hbar\omega_p(0)/2k_B T$ with Planck's constant \hbar , Boltzmann's

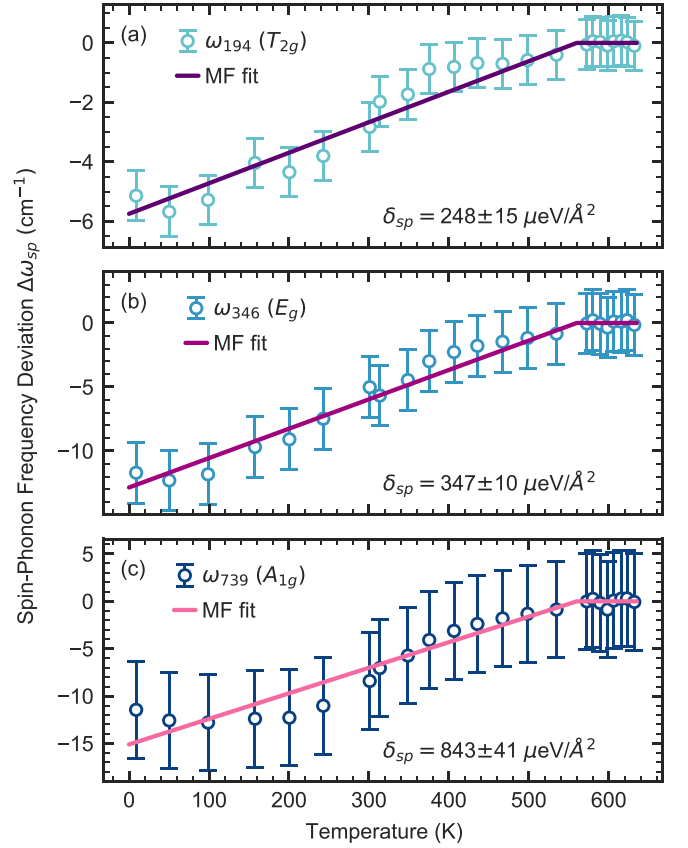


FIG. 3. The measured phonon frequencies are subtracted from the temperature-dependent frequency found with the anharmonic fit [see Figs. 2(b) and 2(c)] to determine $\Delta\omega_{sp}$. Solid lines show fits to the mean-field model which yield the spin-phonon interaction strength δ_{sp} , given in Eq. (7).

constant k_B , and temperature T [21–23]. We fit the peak frequency above 559 K using Eq. (1) to determine $\omega_p(T)$ for each phonon mode. Examples of these fits are shown in Figs. 2(d) and 2(e).

In the magnetically ordered state, the influence of spin order on the phonon frequency can be treated as a small deviation, $\Delta\omega_{sp}$, such that the optical phonon frequency is given as

$$\omega'_p = \omega_p(T) + \Delta\omega_{sp}, \quad (2)$$

where ω'_p is the measured phonon frequency. Then, $\Delta\omega_{sp}$ can be found by taking the difference of the measured frequency and anharmonic temperature-dependent phonon frequency, i.e., $\omega'_p - \omega_p(T)$, as shown in Fig. 3 for selected phonon modes.

Many previous studies of the SPI express the frequency deviation as $\Delta\omega_{sp} = \lambda \langle \mathbf{S}_i \cdot \mathbf{S}_j \rangle$, where λ is a single term capturing the SPI strength and $\langle \mathbf{S}_i \cdot \mathbf{S}_j \rangle$ represents nearest-neighbor spin-correlation function [35–39]. The spin-correlation function can be approximated as $\langle \mathbf{S}_i \cdot \mathbf{S}_j \rangle \approx S_z^2 B_J(T)$, where B_J is the Brillouin function, which has a maximum value of 1 at $T/T_c = 0$ [36]. Thus to find λ without the spin-related, temperature-dependent contribution to the frequency, $\Delta\omega_{sp}$ should be evaluated at $T = 0$. Table I reports frequency deviation measured at 8.8 K, $\Delta\omega_{sp}^0 = \omega'_p - \omega_p(8.8 \text{ K})$, the

TABLE I. Symmetry, spin-phonon frequency deviation, and λ coupling strength of the measured phonon modes in YIG.

Phonon frequency (cm ⁻¹)	Symmetry	Spin-phonon frequency deviation $\Delta\omega_{sp}^0$ (cm ⁻¹)	Coupling strength λ (cm ⁻¹)
174	T_{2g}	8.4 ± 0.9	1.3 ± 0.1
194	T_{2g}	5.1 ± 0.8	0.8 ± 0.1
239	T_{2g}	11.4 ± 1.0	1.8 ± 0.2
276	E_g	3.5 ± 0.6	0.6 ± 0.1
346	E_g	12 ± 2	1.9 ± 0.4
378	T_{2g}	-2.3 ± 4.2	-0.4 ± 0.7
447	T_{2g}	8 ± 4	1.3 ± 0.6
508	E_g	8 ± 2	1.3 ± 0.3
591	T_{2g}	10 ± 3	1.6 ± 0.5
739	A_{1g}	11 ± 5	1.8 ± 0.8

lowest temperature reached in our experiments. The high T_c of YIG and slow decrease of $B_J(T)$ results in $B_J(8.8 \text{ K}) \approx 1$. Then, $\langle \mathbf{S}_i \cdot \mathbf{S}_j \rangle \approx S_z^2$ and using $S_z = \frac{5}{2}$ for the magnetic iron atoms in YIG, λ is found from $\Delta\omega_{sp}^0$, also reported in Table I. Examining the results shown in Table I, there is no clear trend for $\Delta\omega_{sp}^0$ and λ with either the frequency or symmetry of the mode. These results highlight the deficiency of the λ model that has been applied successfully for other materials with a simple unit cell such as FeF₂ and ZnCr₂O [35–39].

IV. DISCUSSION

The simple λ model, which treats all phonon modes equally, is insufficient for describing the SPI in YIG. This is not surprising as the large unit cell leads to complicated phonon dispersions. However, a more detailed first-principles approach like density-functional theory for determining the SPI is exceedingly difficult, again due to the large unit cell of YIG, as well as the especially high precision required in the computations to accurately describe the lattice vibrations and their coupling to magnetic order. Thus, to describe spin-phonon interaction in YIG, we develop a modified mean-field model that captures the mode dependence of the SPI.

We begin with the Ginzburg-Landau (GL) potential describing the magnetic order,

$$F = \frac{A}{2}m^2 + \frac{B}{2}m^4 \quad (3)$$

where $m \equiv M/M_0$ is the ferrimagnetic order parameter defined as the magnetization (M) divided by its zero temperature value (M_0). The GL parameters A and B have units of energy and $A = -a(T_c - T)$, where T_c is the magnetic transition temperature. The temperature dependence of the order parameter agrees well with the temperature dependence of the magnetic moment of YIG reported in the literature (Supplemental Material [34]).

This GL potential only includes magnetic order, and thus needs to be expanded to include phonon contribution to the GL potential. By including only the harmonic terms, the GL potential takes the form

$$F = \frac{A}{2}m^2 + \frac{B}{2}m^4 + \frac{1}{2}\mu\omega u^2 + \frac{1}{2}\delta_{sp}m^2u^2, \quad (4)$$

where μ is the phonon-mode reduced mass, ω is the phonon frequency, u is the atomic displacement, and δ_{sp} is the SPI strength [40,41]. Note that for phonons with irreducible representation A_g and T_{2g} , the symmetry allows a cubic term proportional to m^2u , which is weak in YIG; see Supplemental Material [34,42].

Equilibrium values m_* and u_* are found from the conditions

$$\frac{\partial F}{\partial m} = 0, \quad \frac{\partial F}{\partial u} = 0 \quad (5)$$

and the spin-dependent phonon frequency (Ω) is determined by

$$\mu\Omega^2 = \left. \frac{\partial^2 F}{\partial u^2} \right|_{m=m_*, u=u_*} = \mu\omega^2 + \delta_{sp}m_*^2. \quad (6)$$

Now, using the equilibrium value of $m_* = \sqrt{a(T_c - T)/B}$, Ω is approximately given by

$$\Omega(T) \approx \omega + \frac{\delta_{sp}}{2\mu\omega} \left(1 - \frac{T}{T_c} \right) \quad (7)$$

to first order in δ_{sp} . (Note: δ_{sp} is defined for angular frequencies). Compared to the λ model, we see that the frequency deviation is determined by the frequency and reduced mass of the phonon mode, as well as the SPI strength. We use this improved mean-field theory to extract the SPI strength. Figure 3 shows $\Delta\omega_{sp}$ across the temperature range, with fits using Eq. (7) to extract the δ_{sp} , shown in Fig. 4.

To further understand the SPI found from the modified mean-field model, we examine the atomic displacements of each phonon mode. Using group theory projection operators, we can derive a basis of eigenmodes that brings the

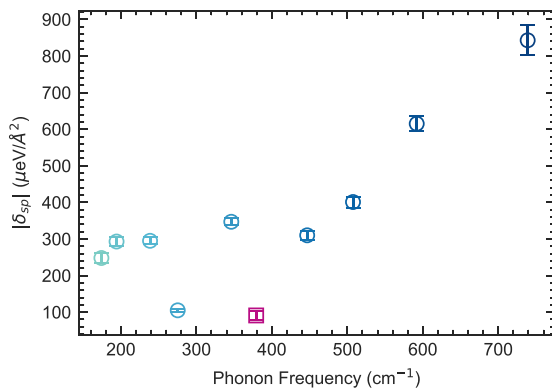


FIG. 4. Absolute value of the spin-phonon interaction strength evaluated with the mean-field model for the phonon modes in YIG. The measured δ_{sp} for the ω_{378} mode is negative (purple square), while the rest of the measured δ_{sp} are positive.

dynamical matrix to a block-diagonal form [43]. The 739-cm⁻¹ mode only involves the O atoms' displacements due to its A_g symmetry (see Supplemental Material [34]). Because it only involves O atoms, this mode has the smallest reduced mass μ compared with T_{2g} and E_g modes. We find that this phonon mode has the largest δ_{sp} . This finding is consistent with the interpretation that the vibrations of the light O atoms are most affected by the magnetic ordering of the heavy Fe atoms. The symmetries of other phonon modes, T_{2g} and E_g , allow motions of all three ion types (Y, Fe, O) in principle. First-principles calculations of the Raman phonon frequencies and symmetries allow us to assign μ to each Raman phonon. We find that, as expected, lower-frequency phonons have larger μ (see Supplemental Material [34]). Using these values of μ to calculate the SPI, we find that higher-frequency phonons have larger SPI as shown in Fig. 4. This trend suggests that the atoms with stronger bonds (consequently higher phonon frequency) are more affected by magnetic ordering.

V. CONCLUSION

In summary, we investigate SPI associated with optical phonon modes of a YIG bulk crystal. By taking polarization-resolved Raman spectra, we analyze their symmetry. Temperature-dependent Raman spectra taken over a broad temperature range of 8.8–635 K allow us to evaluate SPI quantitatively and specific to a particular phonon mode. By developing an improved mean-field model and applying a refined analysis, we discover that the SPI increases with phonon frequency. The A_g mode involving vibrations of only O atoms has the strongest SPI. These results provide both direct and mode-specific interaction strengths, thus providing valuable information for advancing theories of magnetic insulators and for exploring spintronic devices such as those based on spin-caloritronic effects.

ACKNOWLEDGMENTS

This research was primarily supported (J.C., M.R.-V., B.F., J.H., J.Z., G.A.F., and X.L.) by the National Science Foundation through the Center for Dynamics and Control of Materials: an NSF MRSEC under Cooperative Agreement No. DMR-1720595. J.H. acknowledges NSF Grant No. DMR-1729588. G.A.F. acknowledges support from NSF Grant No. DMR-1949701. G.K. and N.A.B. were supported by the Cornell Center for Materials Research: an NSF MRSEC under Cooperative Agreement No. DMR-1719875.

K.S.O. and J.C. performed measurements. B.F. built the experimental system. K.S.O. and J.C. analyzed experimental results. M.R.-V. and G.A.F. developed mean-field model and performed group theory analysis with input from G.K. G.K. and N.A.B. performed first-principles evaluation. J.H. and J.Z. provided and characterized the YIG sample. K.S.O., J.C., M.R.-V., and X.L. wrote the original manuscript. X.L. and G.A.F. supervised the project. All authors assisted in the discussion of results and revision of the manuscript.

-
- [1] V. V. Kruglyak, S. O. Demokritov, and D. Grundler, *J. Phys. D: Appl. Phys.* **43**, 264001 (2010).
- [2] A. A. Serga, A. V. Chumak, and B. Hillebrands, *J. Phys. D: Appl. Phys.* **43**, 264002 (2010).
- [3] A. V. Chumak and H. Schultheiss, *J. Phys. D: Appl. Phys.* **50**, 300201 (2017).
- [4] A. Prakash, B. Flebus, J. Brangham, F. Yang, Y. Tserkovnyak, and J. P. Heremans, *Phys. Rev. B* **97**, 020408(R) (2018).
- [5] L. J. Cornelissen, K. J. H. Peters, G. E. W. Bauer, R. A. Duine, and B. J. van Wees, *Phys. Rev. B* **94**, 014412 (2016).
- [6] K. S. Olsson, K. An, G. A. Fiete, J. Zhou, L. Shi, and X. Li, *Phys. Rev. X* **10**, 021029 (2020).
- [7] H. Hayashi and K. Ando, *Phys. Rev. Lett.* **121**, 237202 (2018).
- [8] X. Zhang, C. L. Zou, L. Jiang, and H. X. Tang, *Sci. Adv.* **2**, e1501286 (2016).
- [9] J. Li, S. Y. Zhu, and G. S. Agarwal, *Phys. Rev. Lett.* **121**, 203601 (2018).
- [10] V. Cherepanov, I. Kolokolov, and V. L'vov, *Phys. Rep.* **229**, 81 (1993).
- [11] A. Prabhakar and D. D. Stancil, *Spin Waves: Theory and Applications* (Springer, New York, 2009), p. 333.
- [12] J. Barker and G. E. W. Bauer, *Phys. Rev. Lett.* **117**, 217201 (2016).
- [13] L. S. Xie, G. X. Jin, L. He, G. E. W. Bauer, J. Barker, and K. Xia, *Phys. Rev. B* **95**, 014423 (2017).
- [14] T. Kikkawa, K. Shen, B. Flebus, R. A. Duine, K. I. Uchida, Z. Qiu, G. E. W. Bauer, and E. Saitoh, *Phys. Rev. Lett.* **117**, 207203 (2016).
- [15] D. A. Bozhko, A. A. Serga, P. Clausen, V. I. Vasyuchka, F. Heussner, G. A. Melkov, A. Pomyalov, V. S. L'vov, and B. Hillebrands, *Nat. Phys.* **12**, 1057 (2016).
- [16] H. Man, Z. Shi, G. Xu, Y. Xu, X. Chen, S. Sullivan, J. Zhou, K. Xia, J. Shi, and P. Dai, *Phys. Rev. B* **96**, 100406(R) (2017).
- [17] D. A. Bozhko, P. Clausen, G. A. Melkov, V. S. L'vov, A. Pomyalov, V. I. Vasyuchka, A. V. Chumak, B. Hillebrands, and A. A. Serga, *Phys. Rev. Lett.* **118**, 237201 (2017).
- [18] S. F. Maehrlein, I. Radu, P. Maldonado, A. Paarmann, M. Gensch, A. M. Kalashnikova, R. V. Pisarev, M. Wolf, P. M.

- Oppeneer, J. Barker, and T. Kampfrath, *Sci. Adv.* **4**, eaar5164 (2018).
- [19] M. Agrawal, V. I. Vasyuchka, A. A. Serga, A. D. Karenowska, G. A. Melkov, and B. Hillebrands, *Phys. Rev. Lett.* **111**, 107204 (2013).
- [20] A. Rückriegel, P. Kopietz, D. A. Bozhko, A. A. Serga, and B. Hillebrands, *Phys. Rev. B* **89**, 184413 (2014).
- [21] R. A. Cowley, *Rep. Prog. Phys.* **31**, 123 (1968).
- [22] M. Balkanski, R. F. Wallis, and E. Haro, *Phys. Rev. B* **28**, 1928 (1983).
- [23] J. Menéndez and M. Cardona, *Phys. Rev. B* **29**, 2051 (1984).
- [24] S. Geller and M. A. Gilleo, *J. Phys. Chem. Solids* **3**, 30 (1957).
- [25] S. Geller and M. A. Gilleo, *J. Phys. Chem. Solids* **9**, 235 (1959).
- [26] G. P. Rodrigue, H. Meyer, and R. V. Jones, *J. Appl. Phys.* **31**, S376 (1960).
- [27] A. B. Harris, *Phys. Rev.* **132**, 2398 (1963).
- [28] M. Wu, *Solid State Phys.* **62**, 163 (2010).
- [29] S. Kimura and I. Shindo, *J. Cryst. Growth* **41**, 192 (1977).
- [30] S. Khanra, A. Bhaumik, Y. D. Kolekar, P. Kahol, and K. Ghosh, *J. Magn. Magn. Mater.* **369**, 14 (2014).
- [31] J. M. Costantini, S. Miro, F. Beuneu, and M. Toulemonde, *J. Phys.: Condens. Matter* **27**, 496001 (2015).
- [32] E. J. J. Mallmann, A. S. B. Sombra, J. C. Goes, and P. B. A. Fechine, *Solid State Phenom.* **202**, 65 (2013).
- [33] A. A. Jalali, S. Kahl, V. Denysenkov, and A. M. Grishin, *Phys. Rev. B* **66**, 104419 (2002).
- [34] See Supplemental Material at <http://link.aps.org/supplemental/10.1103/PhysRevB.104.L020401> for the derivations of the group theory, Raman activity, and mean-field theory, the first principles evaluation of the Raman phonons, and additional examples of the anharmonic and mean-field fits.
- [35] C. J. Fennie and K. M. Rabe, *Phys. Rev. Lett.* **96**, 205505 (2006).
- [36] D. J. Lockwood and M. G. Cottam, *J. Appl. Phys.* **64**, 5876 (1988).
- [37] A. B. Sushkov, O. Tchernyshyov, W. Ratcliff, S. W. Cheong, and H. D. Drew, *Phys. Rev. Lett.* **94**, 137202 (2005).
- [38] D. J. Lockwood, *Low Temp. Phys.* **28**, 505 (2002).
- [39] E. Aytan, B. Debnath, F. Kargar, Y. Barlas, M. M. Lacerda, J. X. Li, R. K. Lake, J. Shi, and A. A. Balandin, *Appl. Phys. Lett.* **111**, 252402 (2017).
- [40] D. Dey, T. Maitra, U. V. Waghmare, and A. Taraphder, *Phys. Rev. B* **101**, 205132 (2020).
- [41] A. Paul, P. Sharma, and U. V. Waghmare, *Phys. Rev. B* **92**, 054106 (2015).
- [42] R. Z. Levitin, A. S. Markosyan, and V. N. Orlov, *Fiz. Tverd. Tela (Leningrad)* **25**, 1861 (1983) [*Sov. Phys. Solid State* **25**, 1074 (1983)].
- [43] M. S. Dresselhaus, G. Dresselhaus, and A. Jorio, *Group Theory* (Springer, Berlin, 2008).